Molecular Electronic Junctions Achieved High Thermal Switch Ratios in Atomistic Simulations

Xingfei Wei[†] and Rigoberto Hernandez[*,†,‡,¶]

†*Department of Chemistry, Johns Hopkins University, Baltimore, Maryland 21218, USA*

‡*Department of Chemical & Biomolecular Engineering, Johns Hopkins University, Baltimore, Maryland 21218, USA*

¶*Department of Materials Science and Engineering, Johns Hopkins University, Baltimore, Maryland 21218, USA*

E-mail: r.hernandez@jhu.edu

Abstract

The development of devices that improve thermal energy management requires thermal regulation with efficiency comparable to the ratios $R \sim 10^5$ in electric regulation. Unfortunately, current materials and devices in thermal regulators have only been reported to achieve $R \sim 10$. We use atomistic simulations to demonstrate that Ferrocenyl (Fc) molecules under applied external electric fields can alter charge states and achieve high thermal switch ratios $R = G_q/G_0$, where G_q and G_0 are the high and low limiting conductances. When an electric field is applied, Fc molecules are positively charged and the SAM-Au interfacial interaction is strong, leading to high heat conductance G_q. On the other hand, with no electric field, the Fc molecules are charge neutral and the SAM-Au interfacial interaction is weak, leading to low heat conductance G_0. We optimized various design parameters for the device performance, including the Au-to-Au gap distance L, the system operation temperature T, the net charge on Fc molecules q, the Au surface charge number Z, and the SAM number N.

We find that G_q can be very large and increases with increasing q, Z, or N, while G_0 is near 0 at $L > 3.0$ nm. As a result, $R > 100$ was achieved for selected parameter ranges reported here.

Keywords

thermal switch, electric field, heat transfer, interface, ferrocene

1 Introduction

Optimizing thermal energy management is important to developing next-generation microelectronics, heating/cooling systems, and phononic computing devices.[1–5] Useful figures of merit for reporting control of heat or electric flow are the rectification ratio, the regulation ratio, or the switch ratio—R ($= G/G'$), where G and G' are the heat or electric conductance in both directions between two different states with G chosen such that $G > G'$. Thermal conductance switch ratios R as high as 13 have been recently reported by Li et al.[6] using an electric field regulated gold-self-assembled monolayer (SAM)-graphene interface and a carboranethiolate SAM molecular junction. Here, we aim to uncover materials with even larger thermal switch ratios.

In 2006, Chang et al.[7] demonstrated one of the earliest thermal rectification devices. They used carbon and boron nitride nanotubes to achieve a rectification ratio of $R = 1.07$. The thermal conductivity of polyethylene (PE) nanofibers was also reported to change by as much as a factor of 12, when switching between crystal and amorphous phases, leading to R as high $R = 2.2$.[8] Recently, Shrestha et al.[9] also experimentally demonstrated that polymer thermal diodes consisting of irradiated-pristine heterogeneous PE nanofibers can achieve $R = 1.5$. In 2018, Ma and Tian[10] found that switching the heat flow directions in bottle brush polymers can induce a heat carrier populations switch from those of diffusive to ballistic behavior, leading to $R = 1.7$ at a temperature gap of 200 K. Recently, we also

showed that a tree polymer structure using PE branches can reach $R = 1.25$ in a level 5 tree.[11,12]

Despite this progress, the development of regulated phononic devices—e.g., thermal diodes, thermal transistors, and thermal switches—are far behind those of electric devices as measured by presently accessible values of R. Indeed, electric rectification ratios of 10^5 or higher are needed for molecular electronics to compete with silicon-based electronic devices.[13] However, currently the most advanced materials and devices can only yield a thermal regulation ratio 3 to 4 orders lower than this. The Nijhuis group developed various organic electronic devices that can reach electric regulation from $R = 10^4$ to 10^5, using various SAM functionalized organic-inorganic interfaces.[14–20] For example, Han et al.[17] reported an electric field driven molecular switch tunneling junction that can reach $R > 10^4$ at a driven voltage of 0.89 V, using methylviologen -S$(CH_2)_1$1M$V^{2+}X_2^-$ thiol molecules. They later reported that a SAM with the 5,6,11,12,17,18-hexaazatrinaphthylene (HATNA) terminal groups reproduces synaptic plasticity properties and can realize Pavlovian learning.[18] This design also demonstrated memristive properties,—viz. the output depends only on the input driving speed and the number of past switching events—which is useful for designing brain-inspired electronic devices.[18] Moreover, they reported that a Ferrocenyl (Fc) terminated alkanethiolate SAM (Fc-C≡C-Fc), can act as a molecular electric diode $R > 10^5$.[16] They posited that the mechanism involves several steps: application of an electric field electrochemically oxidizes the Fc molecules, then the electrostatic interaction enhances the SAM-electrode coupling strength, reducing the SAM-electrode distance, and finally leading to an increase in electron conductance from the enhanced electron tunneling.[16] This mechanism—viz arising from electric field induced strong electrostatic interactions—can also be applied to enhance and regulate thermal transport.[21–24]

One possible strategy for improving thermal switch ratios involves the identification of new or repurposed materials with high electric switch ratios that are amenable to thermal switching. While $MoSe_2$ and WSe_2 are both thermoelectric materials, for example, WSe_2

has better thermoelectric properties than $MoSe_2$.[25] Using a monolayer $MoSe_2$-WSe_2 lateral heterostructure, Zhang et al.[26] developed a device that achieved both electric regulation $R \sim 10^4$ and thermal regulation $R = 1.96$. They found that tuning of lithium intercalation can lead the thermal conductivity of MoS_2 to change by a factor of 2.33 for thin films and 5 for bulk materials.[27] By reversibly regulating lithium intercalation in MoS_2, Sood et al.[28] achieved a switchable thermal transistor with $R \sim 9.375$, and Li et al.[6] reached the aforementioned value of $R = 13$.

In this work, we use molecular dynamics (MD) simulations to demonstrate that the Fc terminated SAM (Fc-C≡C-Fc) introduced by Chen et al.[16] to regulate electricity can also regulate heat conductance across the Au-SAM-Au hetero-junction. By tuning the gap distance between two Au blocks in the hetero-junction, the system temperature, the Fc molecular oxidation/charge state, the Au surface charge density, and the SAM surface number density, we can optimize R for the molecular junction to high values, as reported below.

2 Methods

2.1 Au-SAM-Au hetero-junction model

The simulation model is built according to Chen et al.[16] The overall box size of the structure shown in Fig. 1a is $32.5 \times 3.9 \times 4.5$ nm^3, and periodic boundary conditions are imposed in all 3 dimensions. We use two blocks of FCC Au crystal as the electrode. Both of the left and right side Au blocks shown therein have 18 Au layers with the (111) facet facing the SAM molecules. We leave 20 nm of vacuum space in between the left and right sides to avoid the direct interaction between the two Au blocks. A representative Fc terminated alkanethiolate SAM structure in molecular detail is shown in Fig. 1b. It contains a thiol group, a C15 alkane chain, and a Fc functional group. In the initial structure of the simulation box, we uniformly packed 48 Fc molecules on the Au surface; see Fig. 1c.

The initial Fc SAM structure on the Au(111) surface is shown in Fig. 1d. The initial

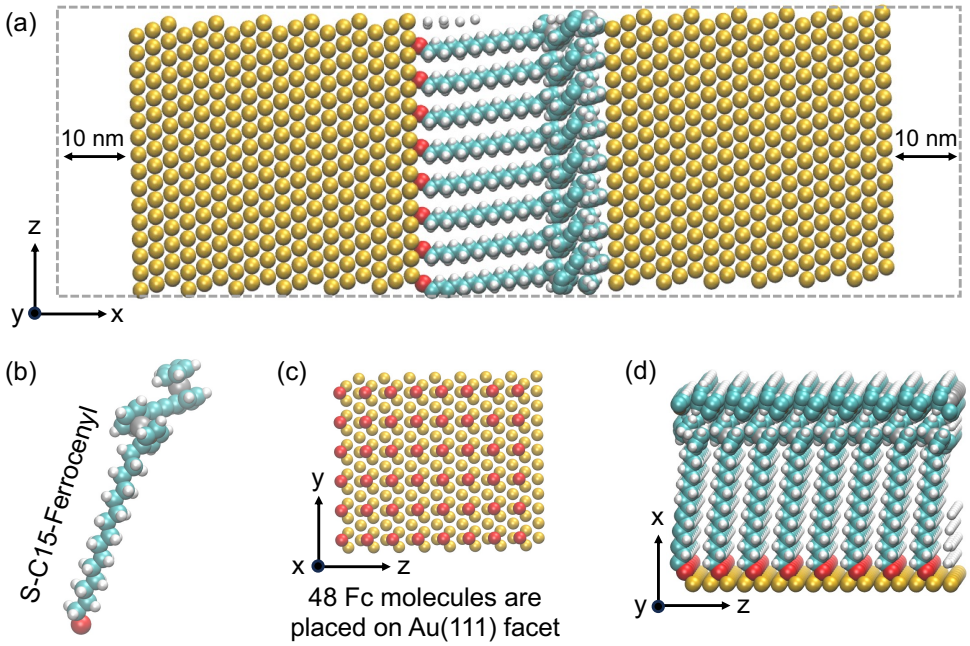

Figure 1: Visual representations of the model employed in this work: (a) The Au-SAM-Au hetero-junction structure, showing the SAM with the thiols bonded to one of the surfaces and the ligands stretched sufficiently to touch the opposite surface. (b) An extended structure of the Fc terminated alkanethiolate. (c) A periodic box of the Au(111) surface shown from above along with 48 uniformly-positioned thiols in the plane just above it. (d) A side view of the initial structure of the SAM with Fcs positioned regularly on a Au(111) surface as shown in panel c.

SAM packing density therein is selected according to the optimum value reported by Chen et al.[16]. To explore the effect of the density of the SAM, we also report cases in which we reduce the SAM number from 48 to 12, by randomly deleting Fc molecules on the Au(111) surface.

The model set up is similar to that in our previous representations of Au-SAM-liquid hard-soft interfaces[23,24,29] and polymer linked gold nanoparticle (AuNP) networks.[11,12] The Fc hetero-junction system construction is based on several simulation models in the literature.[30–33] As in other studies, the Optimized Potentials for Liquid Simulations (OPLS) all-atom force field[34,35] is used to simulate the interactions within Fc molecules. The Au crystal is simulated using the Au-Au Lennard-Jones (LJ) force field of Heinz et al.[36] The cross interaction forces between Au and Fc molecules are described by both LJ and Coulombic interactions with modified parameters from the literature as recorded in the Supporting Information (SI).[37,38] In the Fc SAM molecule, the ethyne linker between two Fc rings is represented as a linear connection.[39]

Our models simulate two different states—viz. positively charged and neutrally charged Fc molecules—to model the electric field regulated Au-SAM-Au hetero-junction.[40] The overall system is charge neutral in both states. Without electric field, both Fc molecules and the Au surface are charge neutral; see Fig. 2a. In this case, the charge neutral Fc molecule force field is adopted from literatures,[41–43] and includes the dihedral angle accounting for rotations of the cyclopentadienyl rings. We can impose an electric field, by setting each Fc molecule to carry $q = +2$e charge, and the unbonded Au layer—viz, the one facing the SAM on the right (or unbonded) slab—carries surface charge $Z = -0.2$ e/atom (Fig. 2b), as was done in Bernardes et al.[44] More generally, we can also vary net charges q on the Fc molecules to represent different oxidation states of the Fc molecules.[44–46] Specifically, we varied $q \in (0.0, 0.4, 0.8, 1.2, 1.6)$ in units of e. In addition, we also varied surface charge Z to allow for variations in the electric field. Specifically, we vary the Au layer surface charge from $Z = -0.05$ to -0.5 e/atom, and report the resulting field strengths. Detailed descriptions

of force field parameters are provided in SI.

Using a polarizable Au surface can affect the thermal transport process across the Au-SAM-liquid interface. Previous work by Gezelter and coworkers[47–50] showed that a polarizable force field can lead to significant thermal conductance differences in AuNP systems,[49,50] but no obvious effect on planar Au interfaces.[48,50] Here, we use an image charge method to model the polarizable planar Au(111) surface[47] and find no difference in the heat conductance as reported below. This is a consequence of the fact that the electric field dominates the observed behavior as it is much larger than the small contributions that can arise from polarizable responses.

2.2 Determining heat conductance from ONEMD simulations

The Large-scale Atomic Molecular Massively Parallel Simulator (LAMMPS) package is used to propagate all MD simulations.[51] The simulation time step is 0.25 fs. The temperature damping parameter is 25 fs for the Langevin thermostat. A buffer size of 2.5 Å is used to reconstruct the neighboring atoms. We use an LJ 12-6 potential with the Lorentz-Berthelot arithmetic combining rule to describe interactions between dissimilar atoms. For both Coulombic and LJ forces, the cutoff radius is 10 Å. Long-range interactions beyond this radius are not included because they did not affect the dynamics or the thermal conductance measurements up to the reported error, while their omission provided significant reduced computational cost.

For simplicity, we use one-way non-equilibrium molecular dynamics (ONEMD)[52,53] to model the heat conduction through the Au-SAM-Au hetero-junction between two fixed layers (as shown in Fig. 2) rather than the more recent reverse non-equilibrium molecular dynamics (RNEMD).[54] The latter avoids the artificial use of the fixed layer in creating a periodic box in which the flux would go in the forward and reverse directions across two respective mirror images of the hetero-junction. However, it appears that the extra calculations needed to perform RNEMD would not lead to significantly different effects,[48–50] and

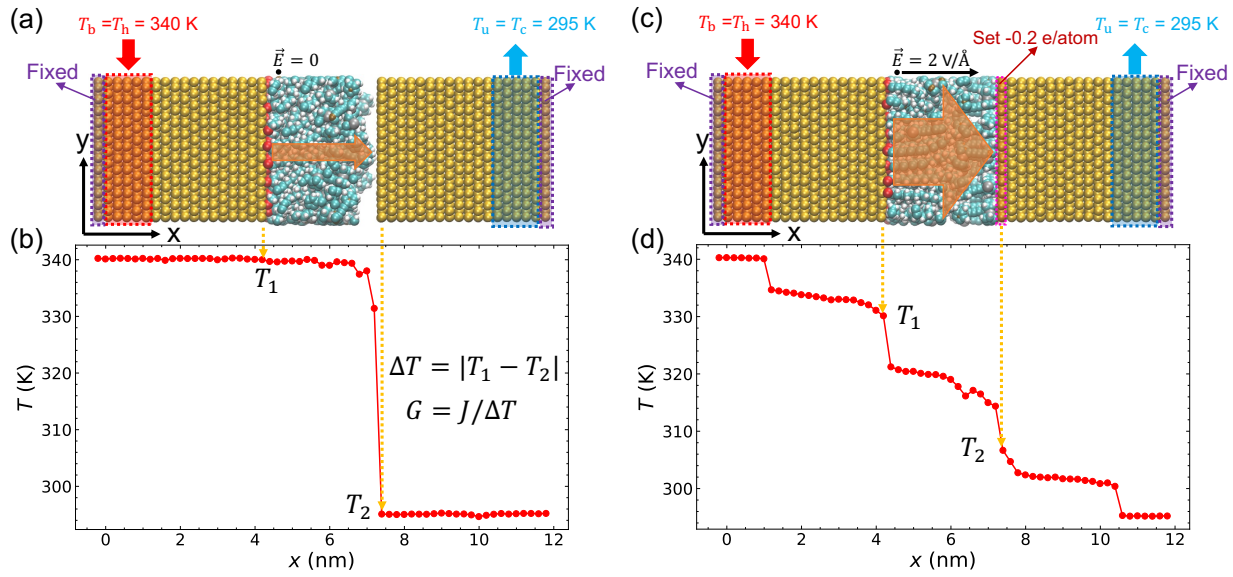

Figure 2: Heat flows from the hot plate (with 5 Au layers on the bonded side) at $T_b = T_h$ to the cold plate (with 5 Au layers on the unbonded side) at $T_u = T_c$ as shown in representative schemes a and c. In between, there are 12 layers of Au, the SAM inside a region of width L = 3.1nm, and another 12 layers of Au, as shown. (The resulting distance between the Au centers at the two fixed layers is 12.34 nm.) In (a), Fc molecules and the Au layers both have net charge zero representing the case when no electric field is 12.34 nm. In (c), each Fc molecule has net charge +2e and the marked Au layer carries $Z = -0.2$ e/atom charge number (b) and (d) show the corresponding temperature profiles, where T_1 and T_2 are the temperatures of the first Au layers on the bonded and unbonded sides, respectively. (Au surface charge density σ = -0.022 e/Å^2 is directly calculated from $Z = -0.2$ e/atom, which emulates the electric field with $E = \sigma/2\varepsilon_0$, and ε_0 is the vacuum permittivity. The corresponding resulting steady-state temperature profiles obtained from MD simulations using the heat conductance method are shown in panels b and d, respectively.

hence can be avoided for the purposes of the current work. The 1st Au layer at each end of the system is fixed, and the subsequent 5 layers constitute a slab thermostatted to set temperatures, where T_{b} and T_{u} are the setting temperatures on the *bonded* slab and *unbonded* slab, respectively. The next 12 Au layers are used to thermalize the temperature distribution on the thermostatted Au slabs, which can avoid the thermostat directly interact with the SAMs.

Initially, the simulation model is relaxed at temperature T = 300 K for 1 - 2 ns by thermostatting all atoms in the two slabs and those in between. The internal thermostats are then turned off for all of the atoms except for the Au atoms in the left and right slabs. The Langevin thermostats on the *bonded* slab—which is on the side of the plate which is bonded to the Fc terminated alkanethiolates—are set at $T_{\mathrm{b}} = T_{\mathrm{h}}$ = 340 K, and the ones on the *unbonded* slab—which is on the side of the plate which is not bonded to the Fc terminated alkanethiolates—are set to $T_{\mathrm{u}} = T_{\mathrm{c}}$ = 295 K. According to Refs. 16,55, the thermal stability of the Fc SAMs is generally good at this temperature range because of the stabilizing interactions between the C12 alkane chain segments. On the other hand, conductive SAMs are less stable as they have been reported to break down at temperatures near 323 K.[56] The ONEMD simulations take about 5 ns to reach steady state when the heat flux between the hot and cold thermostats stabilizes and yields the desired conductance. In what follows, we will report on the heat conductance with varying T_{h} for fixed T_{c}. In addition, the cold temperature T_{c} will be lowered to 95K and 195K to confirm its effect for a given ΔT. T_{h} and T_{c} are the heat and cold temperatures on the system, respectively. We also reversed the temperature settings, T_{h} and T_{c}, to confirm that the heat conductance was the same when the heat flowed from the right (*unbonded*) side to the left (*unbonded*) side. The reported conductances are averages of 6-10 replicates, and represent the flow in both directions in equal proportion.

We determine the temperature distribution across the Au-SAM-Au hetero-junction after they have reached steady state by averaging over the last 2 ns of the ONEMD trajectories.

When no electric field is applied, the Fc SAM molecules and the Au surface are charge neutral. The resulting interaction between the SAM and the Au on the right side is weak because the unstretched ligands are uncharged and the remaining LJ interaction at such distances is small. We thus observe a large temperature gap ($\Delta T = |T_1 - T_2|$) at the interface of Au block at the unbonded side; see Figs. 2a and b. As without electric field, the thermal resistance across the interface of SAMs and the unbonded Au layers is significantly larger than that of the Au layers or SAMs, the temperature profile on the bonded/left side in Fig. 2b seems very flat. When the electric field is applied on the two Au blocks, the Fc SAM molecules are induced to carry positive charges and the Au surface on the right side now carries negative charges. We thus now observe temperature drops (ΔT) across the Au blocks and in between through the Au-SAM-Au junction; see Fig. 2b. The heat flux (J) is calculated from the slope of the accumulative heat at the thermostat; see Fig. S3 in SI. As a result, the heat conductance (G) is directly calculated using $G = J/\Delta T$ in pW/K. For comparison with previous reports, normalized values of G are also reported in MW/m^{2}K in Table S3 in SI relative to the cross sectional area ($S = 17.34$ nm^2).

The gap between the Au blocks in the initial setup reported in Fig. 2 is $L = 3.1$ nm as can be inferred from the figure. This value results from the averaging the centers-of-mass of the mobile Au atoms at the two surfaces for a given distance between the fixed Au atom layers at either side. By varying the latter, we also varied L from 2.5 nm to 3.5 nm to determine the effects of the gap size on the heat conductance and thermal switch performance.

3 Results and discussion

3.1 Heat conductance at different gap distances L

SAM structure at the hetero-junction. Without an applied electric field, as the slabs are moved apart (from $L = 3.0$ nm to L= 3.5 nm), the SAM begins to lose contact with the non-bonded slab as indicated in Fig. 3a. Therein, the interfacial binding interaction is weak

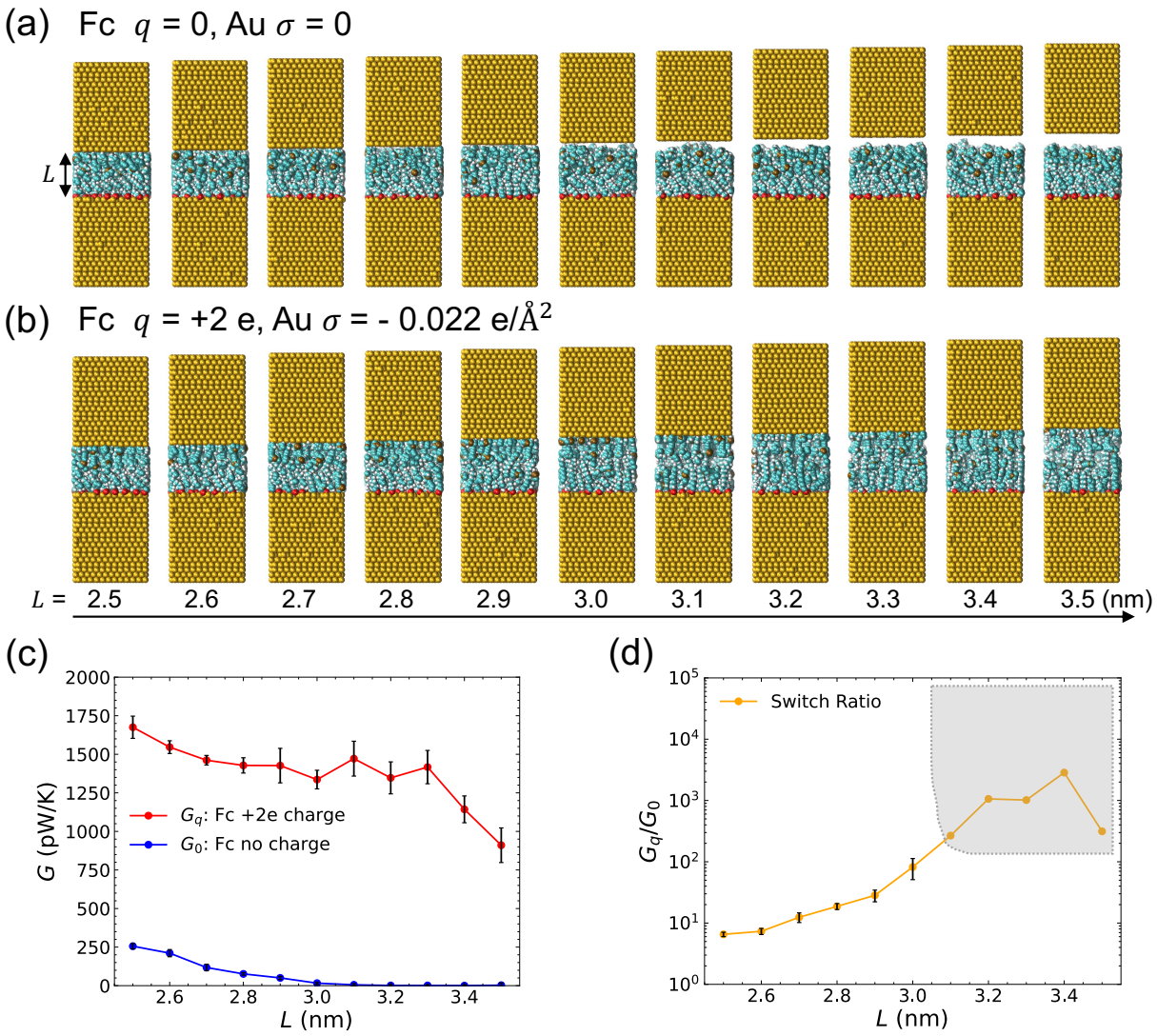

Figure 3: Heat conductances and switch ratios for various Au-to-Au gaps L between the thermostatted layers at the two ends. (a) Representative schemes of Fc SAM for different L, when no electric field is applied and Fc molecules have no net charges. (b) Representative schemes when electric field is applied. Therein, the Au layer has surface charge -0.022 e/Å^2 (-0.2 e/atom) and each Fc molecule has +2e charges. (c) Heat conductances at different L. (d) Thermal switch ratios, $R = G_q/G_0$, at different L, where the error bar is calculated by the relative absolute error. Points in the shaded area have huge uncertainties due to the near zero denominator when G_0 is near 0.

because both the Fc SAM and the Au surface are charge neutral, and hence insufficient to maintain the contact. At $L \lesssim 2.9$ nm, the SAM is in contact with both surfaces, but it is compressed because such gaps are small compared to the SAM's preferred width. As a consequence of the compression, SAMs at this and other small gaps exhibit a mechanical enhancement of the interfacial heat conductance. Under the influence of an electric field, the SAM remains in good contact with the right-side Au surface at gaps with widths up to $L =$ 2.5 to 3.5 nm as indicated in Fig. 3b. Although not reported explicitly, the chains simulated here demonstrated the reduction of chain curling and chain lengthening observed in Refs. 16 and 32 through different order parameters. The Fc SAM and Au surfaces remain close to each other because of the strong electrostatic interactions between the positively-charged Fc SAM molecules and the negatively-charged Au surface. Using this mechanism, Chen et al.[16] developed an electronic molecular junction which can achieve an electric regulation ratio $R \sim 10^5$. The Au-SAM-Au hetero-junction design with Fc molecules introduced here gave rise to even higher thermal switch ratios, $R > 100$, because of the enhancement on the thermal transport[6,23,24,29] due to the electrostatic interaction. Under typical operating conditions, the device can be run with a hotter end relative to the colder end at near ambient temperatures—e.g., at $T_\mathrm{h} = 340$ K and $T_\mathrm{c} = 295$ K—where we see a significant variation in G and R with the gap distance, L; see Fig. 3.

Heat conductance and thermal switch. We see in Fig. 3c that G_q for +2e charged Fc molecules is much larger than the G_0 for charge-neutral Fc molecules. From $L = 3.0$ to 3.5 nm, G_0 is less than 17 pW/K (viz 1.0 MW/m^{2}K) because Fc molecules are charge neutral. In general, values of G_0 have an error bar of ~ 10 pW/K, leading to huge uncertainty in the conductance ratio $R(= G_q/G_0)$ at small G_0. We also find that G_0 increases to 256 pW/K (14.8 MW/m^{2}K) at $L = 2.5$ nm, due to mechanical compression. Meanwhile, when Fc molecules carry net positive charges and the Au surface atoms carry net negative charges, G_q can reach values greater than 1500 pW/K at $L < 3.0$ nm. Although G_0 and G_q both increase, R decreases when L decreases from 2.9 to 2.5 nm; see Figs. 3c and 3d. On the other

hand, in Fig. 3c at $L = 3.4$ and 3.5 nm, we find G_q drops because of the breaking of Au-S chemical bonds at the Au-thiol interface. We also find that G_q is nearly constant at ~ 1400 pW/K (i.e. ~ 80 MW/m^{2}K), from $L = 3.0$ to 3.3 nm with electric field applied. While G_0 is seen to be near 0 at $L \geq 3.1$ nm, its error bar is not quite 0 and almost necessarily larger than the corresponding G_0. This leads to huge relative absolute errors in R. These results suggest that the optimum operation region for the hetero-junction spans from $L = 3.0$ to 3.3 nm, where the thermal switch ratio, R, can achieve values in the range between 100 to 1000; see Fig. 3d. We list G and R across devices with different separation distances L in Table S3 in SI.

The heat conductances in the present models are nearly equal, and take on a value at ~ 80 MW/m^{2}K. This is of the same magnitude reported by Li et al.[6] for carboranethiolate SAM molecular junctions. Our simulation model demonstrates that a thermal switch ratio with $R = 267$ is realizable using the Fc SAM molecular junction at $T_c = 295$ K and $L = 3.1$ nm, which is an order of magnitude higher than $R = 13$ as reported earlier for the carboranethiolate SAM.[6] While we are suggesting the possible heat transfer switching performance of the Fc SAM hetero-junction system based on our simulations alone, it is notable that such a system is realizable as such a design was used earlier by the Nijhuis group[16] in reporting electrical properties.

3.2 Heat conductance for variations in T_c and ΔT

Heat conductance at $T_c = 95$ and 195 K. When the temperature of the cold slab is decreased to $T_c = 95$ or 195 K, we find that the organic SAM molecules shrink due to thermal expansion, and the interfacial contact between the SAM and Au decreases; see schemes in Fig. S4 in SI. At $T_c = 295$ K the interfacial contact is better still, and the thermal conductance is also the highest of the three cases. In general, at the same L, increasing temperature enhances heat conductance for both G_0 and G_q because thermal expansion appears to improve the interfacial interaction; see Fig. 4. At zero electric field and large L (from $L = 3.0$

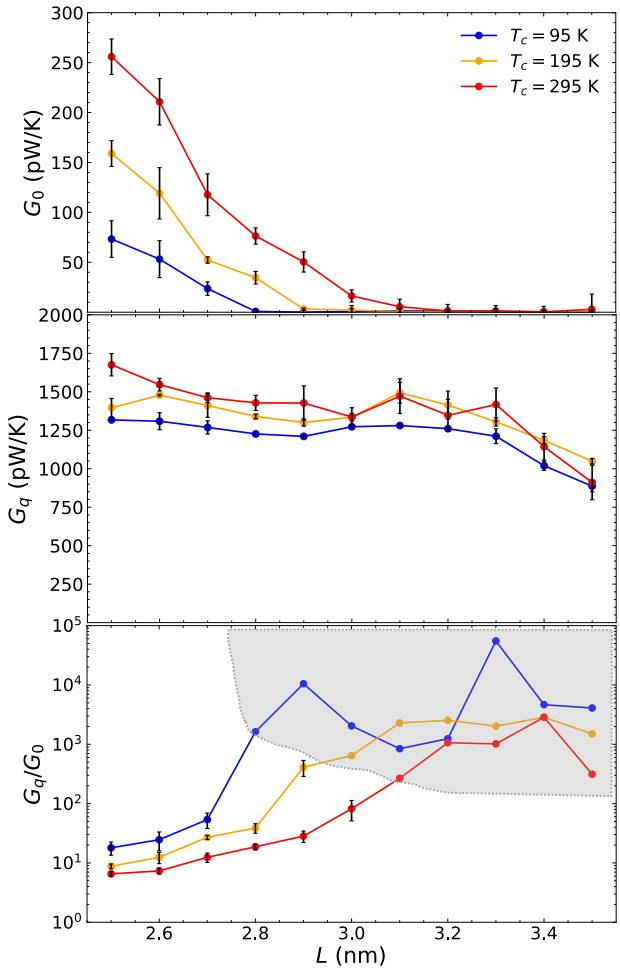

Figure 4: Heat conductance and thermal switch performance at system operation temperatures (T_c = 95, 195, and 295 K), where T_h is set at (T_c + 45) K. Top panel shows heat conductance (G_0) with no charge on Fc molecules and Au surface. Middle panel shows heat conductance (G_q) with charge setting q = +2.0 e on Fc molecules and Z = −0.2 e/atom on the Au surface. Bottom panel shows the thermal switch ratios at different distances L, where the error bar is calculated by the relative absolute error. As in Fig. 3, points in the shaded area have huge uncertainties due to the near zero denominator when G_0 is near 0.

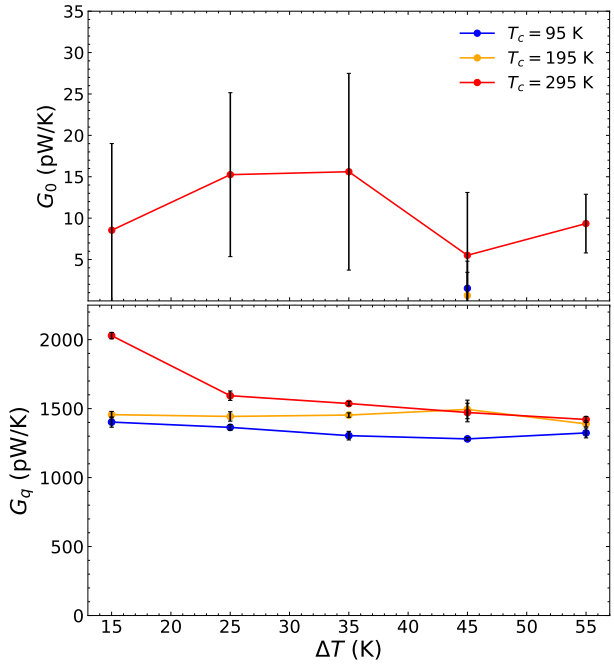

Figure 5: Heat conductance and thermal switch performance at different temperature settings (T_c = 95, 195, and 295 K), where T_h changes from (T_c + 15) to (T_c + 55) K and $\Delta T = T_h - T_c$. Top panel shows the heat conductance (G_0) with no charge on Fc molecules and Au surface. Bottom panel shows the heat conductance (G_q) with the charge set to q = +2.0 e on the Fc molecules and Z = −0.2 e/atom on the Au surface. The error bar is calculated from at least 6 independent runs, which includes 3 left-to-right runs and 3 right-to-left runs. We only report values of G_0 at T_c = 95 and 195 K, for T_h = with ΔT = 45 K. As these values are very small with large uncertainties, G_0 for other ΔT is expected to be similarly trivial

to 3.5 nm), G_0 is small because the interfacial interaction is weak, and the trends in the temperature effect are difficult to discern. Under nontrivial applied electric fields, G_q is very large because the interfacial interaction is strong (as the Fc molecules carry net charges), and the conductance appears to decrease with decreasing temperature. Tables S4 and S5 in SI list G_0 and G_q at $T_c = 95$ K and 195 K for various separation distances L.

Thermal switch at $T_c = 95$ and 195 K. In Sec. 3.1, we reported that the Fc SAM hetero-junction is a thermal switch when the cold slab is held at ambient temperature. When the cold slab temperature decreases to $T_c = 95$ and 195 K, the SAM molecules shrink due to thermal expansion, leading to an increase gap distance between the SAM and the right-side Au surface. As a result, the weak LJ force is further reduced for the charge neutral SAM, and G_0 decreases with decreasing T; see the top panel of Fig. 4. Although G_q also decreases at lower T, we find that the thermal switch ratio, $R = G_q/G_0$, turns out to be larger at lower temperatures; see the bottom panel of Fig. 4. When the hetero-junction is functioning at $T_c = 195$ K, we can achieve $R \sim 1000$, for typical design with $L = 2.9$ to 3.3 nm. When the device is functioning near $T_c = 95$ K, we appear to achieve $R \sim 10^4$ at $L \sim 2.9$ nm and R approaches 10^5 at $L \sim 3.3$ nm. However, in this regime G_0 is near 0, as indicated by the shaded region in Fig. 4 bottom panel, and the accuracy in G_0 reaches the statistical limitations in simulation. The corresponding values in R have large relative absolute errors and they may not be reliable which is what is indicated by the shading. In summary, our simulations suggest that phononic devices—e.g., thermal diodes and thermal transistors—can exhibit comparable logical operation performance as seen in electronic devices. Their confirmation awaits physical realization and measurement.

Variations in T_h and T_c. In order to confirm the robustness of our findings, we apply different temperature gaps between the Au blocks, changing T_h and T_c. For no electric field and 0 net charge on SAM, the top panel in Fig. 5 shows that when changing T_h from 310 to 350 K, while holding T_c fixed at 295 K, G_0 does not depend on T_h. Meanwhile, at $T_c = 295$ K, $G_0 \approx 10$ pW/K which is both small and even smaller with decreasing temperature. The

bottom panel in Fig. 5 also shows that with applied electric field and a net charge of +2e on each Fc molecule, G_q generally does not depend on T_h. One exception occurs when $T_h - T_c = 15$ K at $T_c = 295$ K, where G_q and the thermal switch ratio both slightly increase. In summary, at $T_c = 95$, 195, and 295 K, we find that for many temperature gaps, $T_h - T_c$, (from 5 to 55 K) a Fc Au-SAM-Au hetero-junction with $L \sim 3.0$ nm can achieve robust heat transfer switching performance with $R > 100$.

3.3 Heat conductance for variations in q and Z

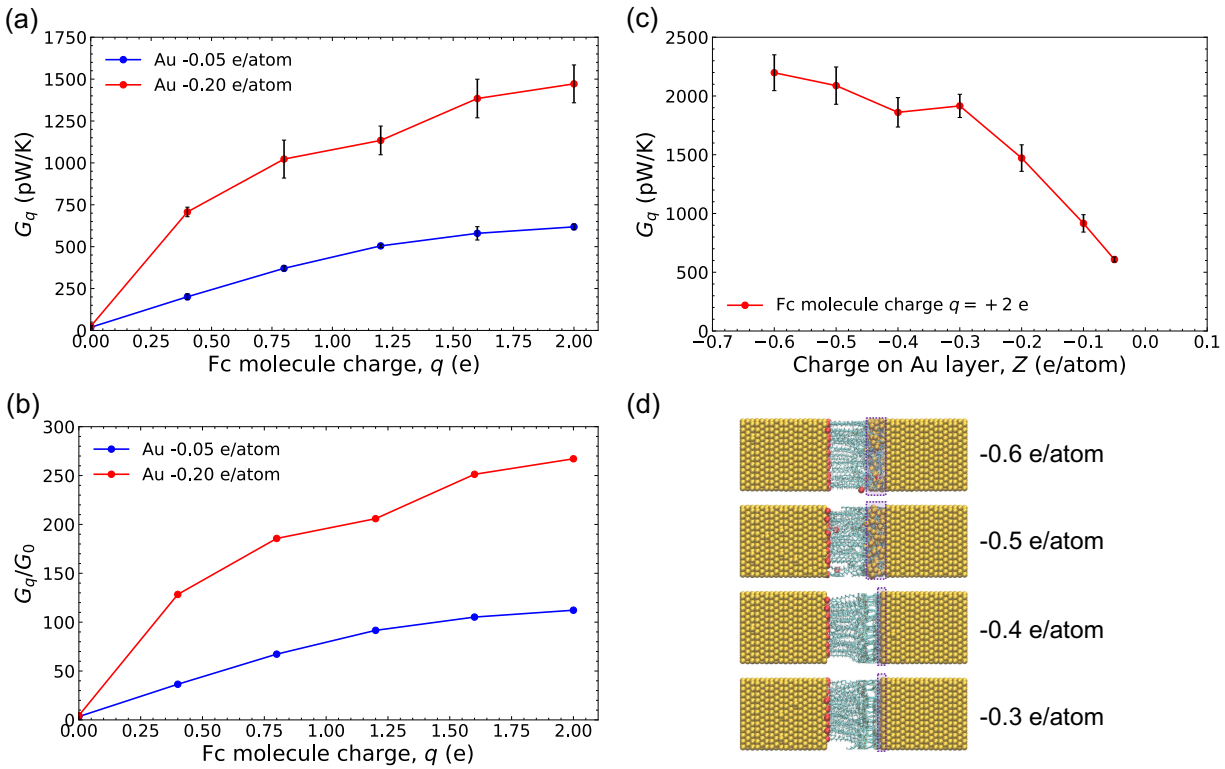

Figure 6: (a) Heat conductances and (b) thermal switch ratios, $R = G_q/G_0$, for different charge settings on the Fc molecule 'q' and on the Au layer 'Z'. (c) Heat conductance at different Z settings with $q = +2$ e. (d) Schemes of the Fc SAM system for $Z = -0.3$ to -0.6 e/atom.

Different oxidation states on Fc molecules. Previous experiment[16] and simulation[44–46] has revealed that the maximum net charge for each Fc molecule is $q = +2$e; see Fig. S1 in SI. In response to electric fields of varying strengths, the oxidation states of the Fc molecules

will also vary and exhibit net charges q lower than +2e. The variations in the resulting heat conductance in the Fc SAM as q is varied is reported in Fig. 6a. We find that G_q decreases with decreasing Fc molecule charge q, but this trend is not linear. When the Au surface charge drops to $Z = -0.20$ e/atom (-0.022 e/Å^2), the heat conductance G_q remains high and the thermal regulation ratio stays high at $R > 100$; see Figs. 6a and 6b. Further reduction of the net charge to $q = 0.0$ leads to significant drops both in G_q to 18.6 pW/K, and R to ~ 4.5. When we apply surface charge density $Z = -0.05$ e/atom, the resulting values of G_q and R are lower than those for $Z = -0.20$ e/atom, but the heat conductance trend is the same. That is, G_q decreases with decreasing q, but R remains nearly constant at a value greater than 100 for $q = 1.6$ and 2.0 e; see Fig. 6a and 6b. Table S6 lists all of the different charge settings (q and Z) on Fc molecules and the Au surface reported here.

Different surface charge settings on the Au layer. The charges on the surface of the Au slab not attached to the SAM determine the charge separation across the device, and hence the surface charge density is directly related to the electric field strength. Following the prior simulation and experiments of Chen et al.[16], we set the surface charge density Au-to-Au distance at $Z = -0.2$ e/atom (-0.022 e/Å^2) and $L = 3.1$ nm as our standard simulation parameters. Figure 6c shows that G_q generally increases with increasing Au surface charge density Z. From $Z = -0.05$ to -0.3 e/atom, the increasing trend of G_q is almost linear. However, at $Z < -0.3$ e/atom, the increase in G_q slows down, because the Au-SAM-Au interface is disrupted and the Au-S bonds begin to break. Representative schemes are shown in Fig. 6d. In our simulation model, the Au-Au interactions are driven only by an LJ force and no Coulombic force. Consequently, the breaking down on the Au surface is due purely to the enhancement of the SAM-Au interaction, but this remains to be verified in real experiments. In actual devices, we expect that when the electric field is too strong, the Au surface of the device will melt, the SAM will disassemble and the Fc molecules may even dissociate.

3.4 Heat conductance for variations in SAM packing density

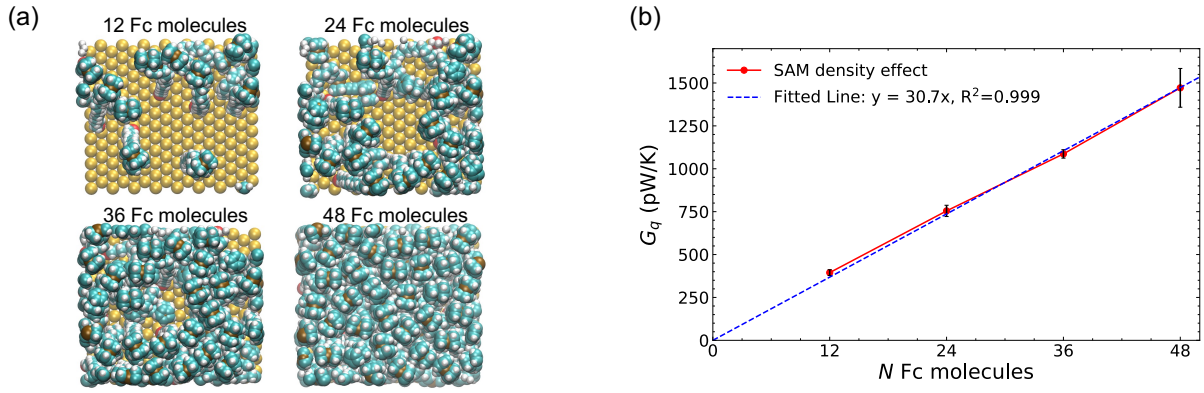

Figure 7: (a) Schemes of different Fc SAM number density on the Au surface. (b) Heat conductance for different numbers of Fc molecules on the Au surface, with $Z = -0.2$ e/atom on the Au layer and $q = +2$ e on the Fc molecules.

Heat conductance at different Fc SAM packing densities. In Fig. 7, we report heat conductance for a range of SAM surface packing densities as high as 2.77 molecules/nm^2 for which Chen et al.[16] reported electric conductance. For example at the largest of these densities, the SAM consists of 48 Fc molecules on a 3.9×4.5 nm^2 Au(111) surface. In experiments, controlling SAM density can be achieved by thermally dissociating the Au-S bonds at high temperatures, or electrical selective desorption of the secondary SAM.[57] We find that with decreasing Fc packing density, the heat conductance G_q also decreases and the trend is mostly linear. The resulting slope is $G_q = 30.7$ pW/K for each Fc molecule contribution. In our previous work,[11] we found that for a single polyethylene chain linked 8 nm diameter large AuNPs, the heat conductance is also about 30 pW/K. Perhaps coincidently, this value of $G_q = 30.7$ pW/K for each Fc molecule is close to single molecular junctions reported in other systems in literature.[11,12,58,59] However, G_0 is very low and its uncertainty is large even at the maximum packing density. As such, the switch ratios, G_q/G_0, and their uncertainties are large, making it difficult to discern quantitative trends. Indeed, mixed Fc with other terminal groups in SAM interfaces were reported by Nijhuis and coworkers.[60] The effect in these mixtures would be particularly interesting because they affect the density

of the Fc molecules, and introduce nonlinear effects due to the interaction with the other ligands. Resolving these effects would constitute a significant new effort that we hope to see in future work. Nevertheless, we performed some simulations of mixed SAMs as reported in the SI. Therein, rather than deleting entire Fc molecules as we did to vary the density in neat SAMs, we modified the would-be deleted Fc molecules by deleting their functional groups and retaining the C12 attached to the substrate. We report in Fig. S5 of the SI that the heat conductance of modified SAM mixtures decreases nonlinearly with the decreasing fraction of Fc molecules in the SAM.

4 Conclusions

In this work, we use all-atom simulation models to demonstrate that a Au-SAM-Au hetero-junction with Fc SAM molecules can achieve thermal regulation ratios of $R > 100$ when subjected to external electric fields, which is perhaps the most significant finding. We also find that heat conductances, G_0 and G_q, increase with decreasing gap distance, L, because of a mechanical compression effect. However, the thermal regulation ratio decreases with decreasing L. Devices with optimal values of $R = G_q/G_0$ are obtained when $L = 3.0$ to 3.3 nm. Outside of that range, the ratio decreases because of the increases in G_0 at $L < 3.0$, and the decreases in G_q at $L > 3.3$. We also find that the hetero-junction can achieve large R when the cold slab is held at below ambient temperatures (as confirmed for $T_c = 95$, 195, and 295 K). Due to thermal expansion, the contact between the Fc SAM and the Au surface is weaker at lower temperatures, which leads to decreasing G_0 and increasing R increase at $T_c = 95$ K. We found that both G_q and R decrease with decreasing oxidation states in the Fc molecules of the SAM. Specifically, we modeled the oxidation state through an effective net charge q on all of the Fc molecules, and measured the resulting heat conductance. We found that G_q increases with increasing electric field strength as effected by the corresponding surface charge Z on the Au surface, when Z is larger than 0.4 e/atom the Fc SAM-Au

interface breaks down. Finally, we found that G_q increases linearly with increasing SAM packing density.

Acknowledgments

This work has been partially supported by the National Science Foundation (NSF) through Grant No. CHE 2102455. The computing resources necessary for this work were performed in part on Expanse at the San Diego Supercomputing Center through allocation CTS090079 provided by Advanced Cyberinfrastructure Coordination Ecosystem: Services & Support (ACCESS), which is supported by National Science Foundation (NSF) grants #2138259, #2138286, #2138307, #2137603, and #2138296. Additional computing resources were provided by the Advanced Research Computing at Hopkins (ARCH) high-performance computing (HPC) facilities.

Supplementary Information

The Supporting Information (SI) includes the following content: detailed information about simulation methods and results.

Data Availability

The data that support the findings of this study are available from the corresponding author upon reasonable request.

References

(1) Li, N.; Ren, J.; Wang, L.; Zhang, G.; Hänggi, P.; Li, B. Colloquium: Phononics: Manipulating Heat Flow with Electronic Analogs and Beyond. *Rev. Mod. Phys.* **2012**,

84, 1045, DOI: 10.1103/RevModPhys.84.1045.

(2) Ding, Y.-F.; Zhu, G.-M.; Shen, X.-Y.; Bai, X.; Li, B.-W. Advances of Phononics in 2012-2022. *Chin. Phys. B* **2022**, *31*, 126301, DOI: 10.1088/1674-1056/ac935d.

(3) Wehmeyer, G.; Yabuki, T.; Monachon, C.; Wu, J.; Dames, C. Thermal Diodes, Regulators, and Switches: Physical Mechanisms and Potential Applications. *Appl. Phys. Rev.* **2017**, *4*, 041304, DOI: 10.1063/1.5001072.

(4) Swoboda, T.; Klinar, K.; Yalamarthy, A. S.; Kitanovski, A.; Muñoz Rojo, M. Solid-State Thermal Control Devices. *Adv. Electron. Mater.* **2021**, *7*, 2000625, DOI: 10.1002/aelm.202000625.

(5) Bathe, M.; Hernandez, R.; Komiyama, T.; Machiraju, R.; Neogi, S. Autonomous Computing Materials. *ACS Nano* **2021**, *15*, 3586–3592, DOI: 10.1021/acsnano.0c09556.

(6) Li, M.; Wu, H.; Avery, E. M.; Qin, Z.; Goronzy, D. P.; Nguyen, H. D.; Liu, T.; Weiss, P. S.; Hu, Y. Electrically Gated Molecular Thermal Switch. *Science* **2023**, *382*, 585–589, DOI: 10.1126/science.abo4297.

(7) Chang, C. W.; Okawa, D.; Majumdar, A.; Zettl, A. Solid-State Thermal Rectifier. *Science* **2006**, *314*, 1121–1124, DOI: 10.1126/science.1132898.

(8) Zhang, T.; Luo, T. High-Contrast, Reversible Thermal Conductivity Regulation Utilizing the Phase Transition of Polyethylene Nanofibers. *ACS Nano* **2013**, *7*, 7592–7600, DOI: 10.1021/nn401714e.

(9) Shrestha, R.; Luan, Y.; Luo, X.; Shin, S.; Zhang, T.; Smith, P.; Gong, W.; Bockstaller, M.; Luo, T.; Chen, R.; Hippalgaonkar, K.; Shen, S. Dual-Mode Solid-State Thermal Rectification. *Nat. Commun.* **2020**, *11*, 1–7, DOI: 10.1038/s41467-020-18212-2.

(10) Ma, H.; Tian, Z. Significantly High Thermal Rectification in An Asymmetric Polymer

Molecule Driven by Diffusive Versus Ballistic Transport. *Nano Lett.* **2018**, *18*, 43–48, DOI: 10.1021/acs.nanolett.7b02867.

(11) Wei, X.; Harazinska, E.; Zhao, Y.; Zhuang, Y.; Hernandez, R. Thermal Transport Through Polymer Linked Gold Nanoparticles. *J. Phys. Chem. C* **2022**, *126*, 18511–18519, DOI: 10.1021/acs.jpcc.2c05816.

(12) Wei, X.; Hernandez, R. Heat Transfer Enhancement in Tree-Structured Polymer Linked Gold Nanoparticle Network. *J. Phys. Chem. Lett.* **2023**, *14*, 9834, DOI: 10.1021/acs.jpclett.3c02367.

(13) Gupta, R.; Fereiro, J. A.; Bayat, A.; Pritam, A.; Zharnikov, M.; Mondal, P. C. Nanoscale Molecular Rectifiers. *Nat. Rev. Chem.* **2023**, *7*, 106–122, DOI: 10.1038/s41570-022-00457-8.

(14) Nerngchamnong, N.; Yuan, L.; Qi, D.-C.; Li, J.; Thompson, D.; Nijhuis, C. A. The Role of van der Waals Forces in the Performance of Molecular Diodes. *Nat. Nanotechnol.* **2013**, *8*, 113–118, DOI: 10.1038/nnano.2012.238.

(15) Yuan, L.; Nerngchamnong, N.; Cao, L.; Hamoudi, H.; Del Barco, E.; Roemer, M.; Sriramula, R. K.; Thompson, D.; Nijhuis, C. A. Controlling the Direction of Rectification in a Molecular Diode. *Nat. Commun.* **2015**, *6*, 6324, DOI: 10.1038/ncomms7324.

(16) Chen, X.; Roemer, M.; Yuan, L.; Du, W.; Thompson, D.; Del Barco, E.; Nijhuis, C. A. Molecular Diodes with Rectification Ratios Exceeding 10^5 Driven by Electrostatic Interactions. *Nat. Nanotechnol.* **2017**, *12*, 797–803, DOI: 10.1038/nnano.2017.110.

(17) Han, Y.; Nickle, C.; Zhang, Z.; Astier, H. P.; Duffin, T. J.; Qi, D.; Wang, Z.; Del Barco, E.; Thompson, D.; Nijhuis, C. A. Electric-Field-Driven Dual-Functional Molecular Switches in Tunnel Junctions. *Nat. Mater.* **2020**, *19*, 843–848, DOI: 10.1038/s41563-020-0697-5.

(18) Wang, Y.; Zhang, Q.; Astier, H. P.; Nickle, C.; Soni, S.; Alami, F. A.; Borrini, A.; Zhang, Z.; Honnigfort, C.; Braunschweig, B.; Thompson, D.; Nijhuis, C. A. Dynamic Molecular Switches with Hysteretic Negative Differential Conductance Emulating Synaptic Behaviour. *Nat. Mater.* **2022**, *21*, 1403–1411, DOI: 10.1038/s41563-022-01402-2.

(19) Liu, R.; Han, Y.; Sun, F.; Khatri, G.; Kwon, J.; Nickle, C.; Wang, L.; Wang, C.-K.; Thompson, D.; Li, Z.-L.; Nijhuis, C. A.; del Barco, E. Stable Universal 1-and 2-Input Single-Molecule Logic Gates. *Adv. Mater.* **2022**, *34*, 2202135, DOI: 10.1002/adma.202202135.

(20) Nijhuis, C. A.; Zhang, Z.; Adoah, F.; Nickle, C.; Karuppannan, S. K.; Wang, L.; Jiang, L.; Tadich, A.; Cowie, B.; Salim, T.; Qi, D.-C.; Thompson, D.; Barco, E. D. Control over Molecular Orbital Gating and Marcus Inverted Charge Transport in Molecular Junctions with Conjugated Molecular Wires. *Adv. Electron. Mater.* **2023**, *9*, 2200637, DOI: 10.1002/aelm.202200637.

(21) Wei, X.; Luo, T. Role of Ionization in Thermal Transport of Solid Polyelectrolytes. *J. Phys. Chem. C* **2019**, *123*, 12659–12665, DOI: 10.1021/acs.jpcc.9b03064.

(22) Wei, X.; Ma, R.; Luo, T. Thermal Conductivity of Polyelectrolytes with Different Counterions. *J. Phys. Chem. C* **2020**, *124*, 4483–4488, DOI: 10.1021/acs.jpcc.9b11689.

(23) Wei, X.; Zhang, T.; Luo, T. Molecular Fin Effect from Heterogeneous Self-Assembled Monolayer Enhances Thermal Conductance Across Hard-Soft Interfaces. *ACS Appl. Mater. Interfaces* **2017**, *9*, 33740–33748, DOI: 10.1021/acsami.7b07169.

(24) Wei, X.; Zhang, T.; Luo, T. Thermal Energy Transport Across Hard-Soft Interfaces. *ACS Energy Lett.* **2017**, *2*, 2283–2292, DOI: 10.1021/acsenergylett.7b00570.

(25) Kumar, S.; Schwingenschlögl, U. Thermoelectric Response of Bulk and Monolayer $MoSe_2$ and WSe_2. *Chem. Mater.* **2015**, *27*, 1278–1284, DOI: 10.1021/cm504244b.

(26) Zhang, Y.; Lv, Q.; Wang, H.; Zhao, S.; Xiong, Q.; Lv, R.; Zhang, X. Simultaneous Electrical and Thermal Rectification in a Monolayer Lateral Heterojunction. *Science* **2022**, *378*, 169–175, DOI: 10.1126/science.abq0883.

(27) Zhu, G.; Liu, J.; Zheng, Q.; Zhang, R.; Li, D.; Banerjee, D.; Cahill, D. G. Tuning Thermal Conductivity in Molybdenum Disulfide by Electrochemical intercalation. *Nat. Commun.* **2016**, *7*, 13211, DOI: 10.1038/ncomms13211.

(28) Sood, A.; Xiong, F.; Chen, S.; Wang, H.; Selli, D.; Zhang, J.; McClellan, C. J.; Sun, J.; Donadio, D.; Cui, Y.; Pop, E.; Goodson, K. E. An Electrochemical Thermal Transistor. *Nat. Commun.* **2018**, *9*, 4510, DOI: 10.1038/s41467-018-06760-7.

(29) Wei, X.; Luo, T. A Phonon Wave Packet Study of Thermal Energy Transport across Functionalized Hard-Soft Interfaces. *J. Appl. Phys.* **2019**, *126*, 015301, DOI: 10.1063/1.5095775.

(30) Nikitina, V. A.; Kislenko, S. A.; Nazmutdinov, R. R.; Bronshtein, M. D.; Tsirlina, G. A. Ferrocene/Ferrocenium Redox Couple at Au(111)/Ionic Liquid and Au(111)/Acetonitrile Interfaces: A Molecular-Level View at the Elementary Act. *J. Phys. Chem. C* **2014**, *118*, 6151–6164, DOI: 10.1021/jp4072108.

(31) Nikitina, V. A.; Kislenko, S. A.; Nazmutdinov, R. R. Understanding the Nature of Heterogeneous Electron Transfer in Molecular and Ionic Solvents: Experiment, Theory, and Computations. *J. Phys. Chem. C* **2019**, *123*, 14370–14381, DOI: 10.1021/acs.jpcc.9b01163.

(32) Goujon, F.; Bonal, C.; Limoges, B.; Malfreyt, P. Description of Ferrocenylalkylthiol SAMs on Gold by Molecular Dynamics Simulations. *Langmuir* **2009**, *25*, 9164–9172, DOI: 10.1021/la9007087.

(33) Zhou, G.; Liu, C.; Bumm, L. A.; Huang, L. Force Field Parameter Development for the

Thiolate/Defective Au(111) Interface. *Langmuir* **2020**, *36*, 4098–4107, DOI: 10.1021/acs.langmuir.0c00530.

(34) Jorgensen, W. L.; Maxwell, D. S.; Tirado-Rives, J. Development and Testing of the OPLS All-Atom Force Field on Conformational Energetics and Properties of Organic Liquids. *J. Am. Chem. Soc.* **1996**, *118*, 11225–11236, DOI: 10.1021/ja9621760.

(35) Kaminski, G. A.; Friesner, R. A.; Tirado-Rives, J.; Jorgensen, W. L. Evaluation and Reparameterization of the OPLS-AA Force Field for Proteins via Comparison with Accurate Quantum Chemical Calculations on Peptides. *J. Phys. Chem. B* **2001**, *105*, 6474–6487, DOI: 10.1021/jp003919d.

(36) Heinz, H.; Vaia, R. A.; Farmer, B. L.; Naik, R. R. Accurate Simulation of Surfaces and Interfaces of Face-Centered Cubic Metals Using 12-6 and 9-6 Lennard-Jones Potentials. *J. Phys. Chem. C* **2008**, *112*, 17281–17290, DOI: 10.1021/jp801931d.

(37) Ahn, Y.; Saha, J. K.; Schatz, G. C.; Jang, J. Molecular Dynamics Study of the Formation of a Self-Assembled Monolayer on Gold. *J. Phys. Chem. C* **2011**, *115*, 10668–10674, DOI: 10.1021/jp200447k.

(38) Rai, B.; P., S.; Malhotra, C. P.; Pradip; Ayappa, K. G. Molecular Dynamic Simulations of Self-Assembled Alkylthiolate Monolayers on an Au(111) Surface. *Langmuir* **2004**, *20*, 3138–3144, DOI: 10.1021/la0357256.

(39) Rego, T.; Silva, G. M.; Goldmann, M.; Filipe, E. J.; Morgado, P. Optimized All-Atom Force Field for Alkynes within the OPLS-AA Framework. *Fluid Phase Equilibria* **2022**, *554*, 113314, DOI: 10.1016/j.fluid.2021.113314.

(40) Nerngchamnong, N.; Thompson, D.; Cao, L.; Yuan, L.; Jiang, L.; Roemer, M.; Nijhuis, C. A. Nonideal Electrochemical Behavior of Ferrocenyl–Alkanethiolate SAMs Maps the Microenvironment of the Redox Unit. *J. Phys. Chem. C* **2015**, *119*, 21978–21991, DOI: 10.1021/acs.jpcc.5b05137.

(41) Lopes, J. N. C.; do Couto, P. C.; da Piedade, M. E. M. An All-Atom Force Field for Metallocenes. *J. Phys. Chem. A* **2006**, *110*, 13850–13856, DOI: 10.1021/jp0628961.

(42) Lousada, C. M.; Pinto, S. S.; Canongia Lopes, J. N.; Minas da Piedade, M. F.; Diogo, H. P.; Minas da Piedade, M. E. Experimental and Molecular Dynamics Simulation Study of the Sublimation and Vaporization Energetics of Iron Metalocenes. Crystal Structures of Fe(η^5-$C_5H_4CH_3)_2$ and Fe[(η^5-(C_5H_5)(η^5-C_5H_4CHO)]. *J. Phys. Chem. A* **2008**, *112*, 2977–2987, DOI: 10.1021/jp7107818.

(43) Bernardes, C. E. S.; Canongia Lopes, J. N.; da Piedade, M. E. M. All-Atom Force Field for Molecular Dynamics Simulations on Organotransition Metal Solids and Liquids. Application to $M(CO)_n$ (M = Cr, Fe, Ni, Mo, Ru, or W) Compounds. *J. Phys. Chem. A* **2013**, *117*, 11107–11113, DOI: 10.1021/jp407739h.

(44) Bernardes, C. E.; Mochida, T.; Lopes, J. N. C. Modeling the structure and thermodynamics of ferrocenium-based ionic liquids. *Phys. Chem. Chem. Phys.* **2015**, *17*, 10200–10208, DOI: 10.1039/C5CP00695C.

(45) Thompson, D.; Larsson, J. A. Modeling Competitive Guest Binding to β-Cyclodextrin Molecular Printboards. *J. Phys. Chem. B* **2006**, *110*, 16640–16645, DOI: 10.1021/jp062553n.

(46) Filippini, G.; Goujon, F.; Bonal, C.; Malfreyt, P. Host–Guest Complexation in the Ferrocenyl Alkanethiols–Thio β-Cyclodextrin Mixed Self-Assembled Monolayers. *J. Phys. Chem. C* **2014**, *118*, 3102–3109, DOI: 10.1021/jp4114128.

(47) Bhattarai, H.; Newman, K. E.; Gezelter, J. D. Polarizable Potentials for Metals: The Density Readjusting Embedded atom Method (DR-EAM). *Phys. Rev. B* **2019**, *99*, 094106, DOI: 10.1103/PhysRevB.99.094106.

(48) Bhattarai, H.; Newman, K. E.; Gezelter, J. D. The Role of Polarizability in the Inter-

facial Thermal Conductance at the Gold–Water Interface. *J. Chem. Phys.* **2020**, *153*, 204703, DOI: 10.1063/5.0027847.

(49) Shavalier, S. A.; Gezelter, J. D. Thermal Transport in Citrate-Capped Gold Interfaces Using a Polarizable Force Field. *J. Phys. Chem. C* **2022**, *126*, 12742–12754, DOI: 10.1021/acs.jpcc.2c01333.

(50) Shavalier, S. A.; Gezelter, J. D. Heat Transfer in Gold Interfaces Capped with Thiolated Polyethylene Glycol: A Molecular Dynamics Study. *J. Phys. Chem. B* **2023**, *127*, 10215–10225, DOI: 10.1021/acs.jpcb.3c05238.

(51) Plimpton, S. J. Fast Parallel Algorithms for Short-Range Molecular Dynamics. *J. Comput. Phys.* **1995**, *117*, 1–19, DOI: 10.1006/jcph.1995.1039.

(52) Müller-Plathe, F. A Simple Nonequilibrium Molecular Dynamics Method for Calculating the Thermal Conductivity. *J. Chem. Phys.* **1997**, *106*, 6082–6085, DOI: 10.1063/1.473271.

(53) Evans, D. J. Homogeneous NEMD Algorithm for Thermal Conductivity—Application of Non-Canonical Linear Response Theory. *Phys. Lett. A* **1982**, *91*, 457–460, DOI: 10.1016/0375-9601(82)90748-4.

(54) Stocker, K. M.; Gezelter, J. D. Simulations of Heat Conduction at Thiolate-Capped Gold Surfaces: The Role of Chain Length and Solvent Penetration. *J. Phys. Chem. C* **2013**, *117*, 7605–7612, DOI: 10.1021/jp312734f.

(55) Cristina, L. J.; Ruano, G.; Salvarezza, R.; Ferrón, J. Thermal Stability of Self-Assembled Monolayers of n-Hexanethiol on Au(111)-(1 × 1) and Au(001)-(1 × 1). *J. Phys. Chem. C* **2017**, *121*, 27894–27904, DOI: 10.1021/acs.jpcc.7b05883.

(56) Park, S.; Kang, S.; Yoon, H. J. Thermopower of Molecular Junction in Harsh Ther-

mal Environments. *Nano Lett.* **2022**, *22*, 3953–3960, DOI: 10.1021/acs.nanolett.2c00422.

(57) Park, B.-W.; Yoon, D.-Y.; Kim, D.-S. Formation and Modification of a Binary Self-Assembled Monolayer on a Nano-Structured Gold Electrode and Its Structural Characterization by Electrochemical Impedance Spectroscopy. *Journal of Electroanalytical Chemistry* **2011**, *661*, 329–335, DOI: 10.1016/j.jelechem.2011.08.013.

(58) Dinpajooh, M.; Nitzan, A. Heat Conduction in Polymer Chains with Controlled End-to-End Distance. *J. Chem. Phys.* **2020**, *153*, 164903, DOI: 10.1063/5.0023085.

(59) Dinpajooh, M.; Nitzan, A. Heat Conduction in Polymer Chains: Effect of Substrate on the Thermal Conductance. *J. Chem. Phys.* **2022**, *156*, 144901, DOI: 10.1063/5.0087163.

(60) Li, Y.; Wang, D.; Peng, W.; Jiang, L.; Yu, X.; Thompson, D.; Nijhuis, C. A. Large Cooperative Effects in Tunneling Rates across van der Waals Coupled Binary Self-Assembled Monolayers. *Nano Today* **2022**, *44*, 101497, DOI: 10.1016/j.nantod.2022.101497.

TOC Graphic